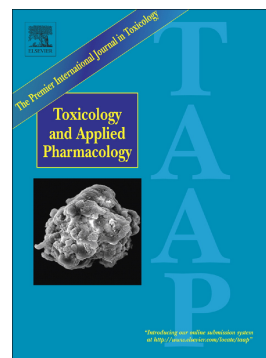


Journal Pre-proof

PCC0208023, a potent SHP2 allosteric inhibitor, imparts an antitumor effect against KRAS mutant colorectal cancer

Xiao Chen, Fangxia Zou, Zhengping Hu, Guangying Du, Pengfei Yu, Wenyan Wang, Hongbo Wang, Liang Ye, Jingwei Tian



PII: S0041-008X(20)30143-5

DOI: <https://doi.org/10.1016/j.taap.2020.115019>

Reference: YTAAP 115019

To appear in: *Toxicology and Applied Pharmacology*

Received date: 28 March 2020

Accepted date: 21 April 2020

Please cite this article as: X. Chen, F. Zou, Z. Hu, et al., PCC0208023, a potent SHP2 allosteric inhibitor, imparts an antitumor effect against KRAS mutant colorectal cancer, *Toxicology and Applied Pharmacology* (2019), <https://doi.org/10.1016/j.taap.2020.115019>

This is a PDF file of an article that has undergone enhancements after acceptance, such as the addition of a cover page and metadata, and formatting for readability, but it is not yet the definitive version of record. This version will undergo additional copyediting, typesetting and review before it is published in its final form, but we are providing this version to give early visibility of the article. Please note that, during the production process, errors may be discovered which could affect the content, and all legal disclaimers that apply to the journal pertain.

© 2019 Published by Elsevier.

**PCC0208023, a potent SHP2 allosteric inhibitor, imparts an antitumor effect
against KRAS mutant colorectal cancer**

Xiao Chen^{1, #}, Fangxia Zou^{1, #}, Zhengping Hu², Guangying Du¹, Pengfei Yu², Wenyan Wang¹, Hongbo Wang¹, Liang Ye^{2, *}, Jingwei Tian^{1, *}

¹School of Pharmacy, Key Laboratory of Molecular Pharmacology and Drug Evaluation (Yantai University), Ministry of Education, Collaborative Innovation Center of Advanced Drug Delivery System and Biotech. Drugs in Universities of Shandong, Yantai University, Yantai 264005 (P.R. China)

²School of Public Health and Management & Institute of Toxicology, Binzhou Medical University, Yantai, 264003, China

Correspondence:

*Liang Ye, Degree: PhD. Tel.: +86-535-6913218; Fax: +86-535-6913218; E-mail: project0088@hotmail.com, School of Public Health and Management & Institute of Toxicology, Binzhou Medical University, Yantai, 264003, China

*Jingwei Tian, Degree: PhD. Tel.: +86-535-6913218; Fax: +86-535-6913218; E-mail: ytupharmlab@163.com; School of Pharmacy, Key Laboratory of Molecular Pharmacology and Drug Evaluation (Yantai University), Ministry of Education, Collaborative Innovation Center of Advanced Drug Delivery System and Biotech. Drugs in Universities of Shandong, Yantai University, Yantai 264005 (P.R. China)

[#] These authors contributed equally to this work.

Abstract

The non-receptor tyrosine phosphatase SHP2, encoded by *PTPN11*, plays an indispensable role in tumors driven by oncogenic KRAS mutations, which frequently occur in colorectal cancer. Here, PCC0208023, a potent SHP2 allosteric inhibitor, was synthesized to evaluate its inhibitory effects against the SHP2 enzyme, and the KRAS mutant colorectal cancer *in vitro* and *in vivo*, and the RAS/MAPK pathway. Consistent with an allosteric mode of inhibition, PCC0208023 can non-competitively inhibit the activity of full-length SHP2 enzyme, but lacks activity against the free catalytic domain of SHP2. Furthermore, PCC0208023 inhibited the proliferation of KRAS mutation-driven human colorectal cancer cells by inhibiting the RAS/ERK signaling pathway *in vitro*. Importantly, PCC0208023 displayed good anti-tumor efficacy against KRAS-driven LS180 and HCT116 xenograft models in nude mice with the decreased Ki67 and p-ERK level, and increased cleaved caspase-3 expression in tumors. Interestingly, PCC0208023 maintained high levels in LS180 tumors within 24 h after administration and was mainly distributed in both intestines and lungs. Molecular docking studies revealed a higher affinity of PCC0208023 with key residues in the SHP2 allosteric pocket than RMC-4550. PCC0208023 deserves further optimization to identify additional low-toxic and potent SHP2 allosteric inhibitors with novel scaffolds for the treatment of patients with KRAS mutation-positive colorectal cancer.

Keywords: PCC0208023; SHP2; allosteric inhibitor; colorectal cancer; KRAS

1 Introduction

Colorectal cancer (CRC) is one of the most commonly diagnosed cancers worldwide with more than 1.8 million new cancer cases and 881,000 deaths in 2018 (Bray et al., 2018; Lee et al., 2018; Shi et al., 2018). About one fourth of patients are diagnosed with metastatic CRC (mCRC). Although the standard treatment using a combined chemotherapy with either an anti-epidermal growth factor receptor (EGFR) agent (cetuximab or panitumumab) or an antiangiogenic agent (bevacizumab or aflibercept) has been used, low response rates have restricted to the use of targeted drugs due to inherent heterogeneity in mCRC (Liang and Shen, 2019). Several studies have shown that KRAS gene mutations occur in 40% of mCRC patients and are considered as negative predictive factors for response to treatment of anti-EGFR or antiangiogenic therapies (Matozaki et al., 2009; Cox et al., 2014; Torres-Ayuso et al., 2018). However, the inhibitors targeting KRAS-driven tumors MRTX849 (Hallin et al., 2019) and AMG 510 (Canon et al., 2019) are in Phase 1/2 clinical trials, and their efficacies have yet to be verified.

Deregulation of the RAS/MAPK signaling pathway drives the growth of human cancer (Dhillon et al., 2007; Matozaki et al., 2009). KRAS, the most frequent mutation (such as G12C), activates the oncogenic RAS/MAPK signaling pathway. KRAS proteins are small GTP-binding proteins that cycle between an active GTP-bound form and an inactive GDP-bound form (Lito et al., 2016; Nussinov et al., 2019). GTP-binding KRAS can upregulate the expression of growth factors and transcription factors that are known to promote cell cycle progression

(Pylayeva-Gupta et al., 2011) and lead to uncontrolled cell proliferation (Mai and Lito, 2018).

SH2 domain-containing protein-tyrosine phosphatase-2 (SHP2), encoded by the *PTPN11* gene, is the first discovered oncogenic tyrosine phosphatase and is overexpressed in different types of cancers (Matozaki et al., 2009; Grossmann et al., 2010; Zhang et al., 2015). SHP2 contains two SH2 domains (N-SH2 and C-SH2), a catalytic (PTP) domain, and a C-terminal tail with two tyrosine phosphorylation sites (Grossmann et al., 2010; Ran et al., 2016). At the basal state, the N-SH2 domain interacts with the PTP domain, resulting in autoinhibition of PTP activity. Upon stimulation of cells, the binding of SHP2 via its SH2 domains to tyrosine phosphorylated growth factor receptors or docking proteins, however, disrupts this intramolecular interaction, which in turn leads to exposure of the PTP domain and allows substrate access to the catalytic site of PTP (Grossmann et al., 2010). Multiple receptor tyrosine kinases (RTKs) act on SHP2, which integrate growth factor signals to promote RAS activation (Nichols et al., 2018). It is generally acknowledged that SHP2 plays an essential role in oncogenic KRAS-driven tumors (Ruess et al., 2018). Genetic knockdown or pharmacological inhibition of SHP2 decreases oncogenic RAS/ERK signaling and cancer growth by disrupting SOS1-mediated RAS-GTP loading (Nichols et al., 2018).

Since SHP099 and RMC-4550 were reported as the first two allosteric SHP2 inhibitors with known structures (Chen et al., 2016; Nichols et al., 2018), numerous SHP2 inhibitors have been reported and only RMC-4630 (NCT03989115, 2019),

TNO155 (NCT03114319, 2017), and JAB-3068 (NCT03518554, 2018) (structures are not disclosed) have entered clinical trials. Notably, Novartis reported a novel class of allosteric SHP2 inhibitors with N-azaspirocycloalkane substituted N-heteroaryl motif, such as NI-1 (Chen et al., 2015). In this article, to obtain more active and drug-like compounds with new scaffolds, we used NI-1 as the template compounds, employed a scaffold-hopping strategy, designed PCC0208023 with 3,6-disubstituted pyrazolo [3,4-b] pyrazine scaffold. The disclosed structures of NI-1 and PCC0208023 are presented (**Scheme 1**).

In the present study, PCC0208023 was synthesized to investigate their inhibitory effects against SHP2 enzyme, the KRAS-mutant CRC *in vitro* and *in vivo*, and the RAS/MAPK signaling pathway. Meanwhile, the pharmacokinetics in LS180 tumor-bearing mice and tissue distribution profiles in rats were also observed.

2 Materials and methods

2.1 Drugs and Chemicals

PCC0208023 (**Scheme 2**) and RMC-4550 (**Scheme 3**) were synthesized by WuXi Apptec (Shanghai, China) Co., Ltd.

2.1.1 Synthesis of PCC0208023

The general route for the synthesis of PCC0208023 was depicted in **Scheme 2**.

2.1.1.1 (4S)-8-(3-Iodo-1-(tetrahydro-2H-pyran-2-yl)-1H-pyrazolo [3,4-b] pyrazin-6-yl)-2-oxa-8-azaspiro [4.5] decan-4-amine (1)

A mixture of compound RM (30.0 g, 82.29 mmol, 1.00 eq), (S)-2-oxa-8-azaspiro [4, 5] decan-4-amine (18.9 g, 82.3 mmol, 1.00 eq) K₂CO₃ (45.5 g, 329 mmol, 4.00 eq) in

NMP (300 mL) was stirred at 80°C for 12 h. The mixture was poured into H₂O (1,000 mL) and extracted with CH₂Cl₂ (300 mL*3), the combined organic phase was washed with H₂O (300 mL*3), brine (300 mL), dried over anhydrous Na₂SO₄, and concentrated under reduced pressure to afford the crude product. The crude was purified by chromatography column (SiO₂, CH₂Cl₂: MeOH = 50:1~10:1) to afford intermediate 1 (25.0 g, 57.1% yield, 91.0% purity) as a white solid. ¹H NMR (400 MHz, CDCl₃): δ 8.19 (s, 1H), 5.80-5.76 (m, 1H), 4.26-4.15 (m, 4H), 3.88-3.85 (m, 1H), 3.80-3.75 (m, 2H), 3.53-3.51 (m, 1H), 3.33-3.30 (m, 2H), 3.23-3.22 (m, 1H), 2.63-2.60 (m, 1H), 2.15-2.14 (m, 1H), 1.95-1.62 (m, 6H).

2.1.1.2 (4S)-8-(3-((2, 3-Dichlorophenyl) thio)-1-(tetrahydro-2H-pyran-2-yl)-1H-pyrazolo [3,4-b] pyrazin-6-yl)-2-oxa-8-azaspiro [4.5] decan-4-amine (2)

A mixture of intermediate 1 (25.0 g, 51.6 mmol, 1.00 eq), 2,3-dichlorobenzenethiol (23.1 g, 129 mmol, 2.50 eq), K₂CO₃ (21.4 g, 155 mmol, 3.00 eq), ethane-1,2-diol (6.41 g, 103 mmol, 2.00 eq), CuI (14.8 g, 77.4 mmol, 1.50 eq), DIPEA (13.3 g, 103 mmol, 18.0 mL, 2.00 eq) in i-PrOH (300 mL) was stirred at 110°C (oil temperature) for 12 h. Then, the mixture was poured into CH₂Cl₂ (1.5 L), the mixture was filtered, and the filtrate was concentrated under reduced pressure to afford the crude product. The crude was purified by chromatography column (SiO₂, CH₂Cl₂: MeOH = 50:1~10:1) to yield intermediate 2 (19.0 g, 67.2% yield, 97.8% purity) as a yellow solid.

2.1.1.3 (S)-8-(3-((2, 3-Dichlorophenyl) thio)-1H-pyrazolo [3,4-b]

**pyrazin-6-yl)-2-oxa-8-azaspiro [4.5] decan-4-amine hydrochloride
(PCC0208023)**

Intermediate 2 in HCl/1, 4-dioxane (4 M, 100 mL) and MeOH (100 mL) was stirred at 20°C for 12 h. The mixture was concentrated under reduced pressure to afford the crude product. The crude was purified by chromatography column (SiO₂, CH₂Cl₂: MeOH = 20:1~7:1) to afford PCC0208023 (I-3 HCl salt) (5.00 g, 31.2% yield) as a yellow solid. ¹H NMR (400 MHz CD₃OD): δ 8.38 (s, 1H), 7.53 (d, J = 8.0 Hz, 1H), 7.05 (t, J = 8.0 Hz, 1H), 6.71-6.69 (m, 1H), 4.47-4.43 (t, 2H), 4.21-4.20 (m, 1H), 4.01 (d, J = 9.2 Hz, 1H), 3.94 (d, J = 9.2 Hz, 1H), 3.25 (dd, J₁ = 2.4 Hz, J₂ = 10.8 Hz, 1H), 3.61-3.60 (m, 1H), 3.41-3.30 (m, 2H), 1.90-1.77 (m, 4H). MS (m/z): 451.0 [M]⁺. HPLC purity: 100%.

2.1.2 Synthesis of RMC-4550

RMC-4550 was synthesized according to Revolution medicines Inc.'s patent (Joglekar et al., 2018) and the general route was depicted in **Scheme 3**. Briefly, 6-bromo-3-chloro-5-methylpyrazine-2-carboxylate was reacted with (2, 3-dichlorophenyl) boric acid under Pd (dppf) Cl₂/K₂CO₃ at 100°C to afford the intermediate 1. Thereafter, intermediate 1 was reacted with (3S, 4S)-3-methyl-2-oxa-8-azaspiro [4.5] decan-4-amine in DMA using DIPEA as a catalyst and heated to 55°C overnight to give the intermediate 2. Finally, DIBAL-H in DCM was added dropwise to a stirred solution of 2 in DCM and kept at -78°C for 30 min. The mixture was warmed, separated, and extracted to give the reference drug RMC-4550. ¹H NMR: ES10608-12-P1B 400 MHz MeOD 7.63 (dd, J₁ = 1.6 Hz, J₂ =

8.0 Hz, 1H), 7.41 (t, $J = 7.6$ Hz, 1H), 7.34 (dd, $J_1 = 1.2$ Hz, $J_2 = 8.0$ Hz, 1H), 7.67 (s, 2H), 4.26–4.23 (m, 1H), 3.86 (d, $J = 8.8$ Hz, 1H), 3.73 (d, $J = 8.8$ Hz, 1H), 3.61–3.57 (m, 2H), 3.18–3.03 (m, 3H), 2.24 (s, 3H), 1.98–1.89 (m, 2H), 1.87–1.70 (m, 2H), 1.23 (d, $J = 6.8$ Hz, 1H). MS (m/z): 437.0 $[M+H]^+$. HPLC purity: 100%.

2.2 Reagents

Antibodies against SHP2 (#3397), p-SHP2 (#3751), MEK1/2 (#4694), p-MEK1/2 (#9154), ERK1/2 (#4696), p-ERK1/2 (#4376), cleaved caspase-3 (#9664), Ki67 (#9027), and GAPDH (#5174) were obtained from Cell Signaling Technology. Antibody against recombinant human SHP2 protein (ab42578) was obtained from Abcam. SHP-2, His-Tag (#79018) was from BPS Bioscience. Bisphosphorylated insulin receptor substrate 1 (IRS-1) peptide (P16778) was from Sangon Biotech. EnzChek[®] Phosphatase Assay Kit (#E12020) was from Invitrogen. Cell Counting Kit-8 (CCK-8) (C0040), methylthiazolyldiphenyl-tetrazolium bromide (MTT) (ST316), penicillin streptomycin solution (C0222), enhanced BCA protein assay kit (P0009), ultra-sensitive ECL chemiluminescence kit (P0018AS), and crystal violet staining solution (C0121) were from Beyotime Biotechnology. RPMI 1640 medium (11875093), Leibovitz's L-15 medium (11415064), McCoy's 5A medium (16600082), and fetal bovine serum (10099141) were purchased from Gibco. Epidermal growth factor (EGF) (354052) and Matrigel[®] (356234) were obtained from Corning Inc. The RAS Pull-down Activation Assay Biochem Kit (BK008) was purchased from Cytoskeleton Inc.

2.3 SHP2 inhibition assay

The experiment was based on the reaction of the SHP2 enzyme (full-length and catalytic domain) and the substrate DIFMUP (6, 8-difluoro-4-methylumbelliferyl phosphate). The SHP2 enzyme (full-length and catalytic domain) removes a phosphate group from DIFMUP, resulting in the generation of fluorescent DIFMU. SHP2 enzymatic activity can be determined by a change in fluorescence intensity. The assay was performed as previously described (Chen et al., 2016), which was conducted by Pharmaron Inc. (Beijing, China). RMC-4550 and PCC0208023 were three-fold serially diluted from 4 or 20 mM for 10 doses in DMSO. Then, 50 μ L of the compound dilutions were transferred into each well of the assay plate and then sealed and centrifuged at 1,000 rpm for 1 min. Then, 10 μ L of the 2 \times SHP2 (full-length) and 2 \times bisphosphorylated insulin receptor substrate 1 (IRS-1) peptide mixture were prepared in a chilled assay buffer and then added into each well of the assay plate, sealed, and centrifuged at 1,000 rpm for 1 min. The reaction was then initiated by adding 10 μ L of 2 \times DIFMUP to each well of the assay plate and measuring the fluorescence signal after 2 h on an Envision 2104 plate reader. The inhibition assay conditions for the SHP2 catalytic domain were identical except for the activating peptide that was excluded and the fluorescent signal was measured overnight.

2.4 Inhibition types of SHP2

In the experiment, the final concentrations of RMC-4550 were 5 nM, 10 nM, and 20 nM, and the final concentrations of PCC0208023 were 2 nM, 4 nM, and 8 nM. The experimental procedure was analogous to the SHP2 enzymatic activity assay, except

for the fluorescence signal was measured for 60 min with an interval of 2 min on an Envision 2104 plate reader.

2.5 Cell lines and cell culture

LS180 and HCT116 colon cells were purchased from the Type Culture Collection of the Chinese Academy of Sciences (Shanghai, China). The cancer cell lines SW837 and SW1463 were originated from the American Type Culture Collection (ATCC). LS180 colon cells were cultured in RPMI 1640 medium, HCT116 cells in McCoy's 5A medium, and all other human cell lines in Leibovitch's L-15 medium, supplemented with 10% fetal bovine serum (FBS) and 1% penicillin-streptomycin. The LS180 and HCT116 cells were cultured in a humidified incubator at 37°C with 5% CO₂, whereas SW837 and SW1463 cells at 37°C with 100% air. The mutation states of the cancer cell lines used in the experiments were shown in **Table 1**.

2.6 Cell viability assay

Cell viability was assessed using the MTT assay and CCK-8 assay as previously reported (Lv et al., 2017). Briefly, cancer cells (**Table 1**) were cultured and seeded in 96-well microplates at a density of 800–8,000 cells per well and allowed to adhere overnight in complete growth media. Cancer cells were treated with different concentrations of RMC-4550 (1.56, 3.12, 6.25, 12.5, 25, and 50 μ M) or PCC0208023 (0.25, 0.5, 1, 2.5, 5, and 10 μ M). Control cells were treated with DMSO (final concentration = 0.1%). In accordance with manufacturer's protocol, cell viability of HCT116 cell was assessed at 3, 5, and 7 days ($n = 3$) by the MTT assay, and that of LS180, SW837, and SW1463 cells were assessed at 3, 5 and 7 days ($n = 3$) by the

CCK-8 assay. All data represented the average of at least three independent experiments.

2.7 Colony formation assay

SW1463 and SW837 cells were plated onto six-well plates at a density of 500–1,000 cells per well, depending on growth rate (Li et al., 2019). After 24 h, the cells were treated with PCC0208023 using various concentrations (SW837: 0.15, 0.5, 1.5 μM ; SW1463: 0.25, 0.5, 0.75 μM), cultured for 15–21 days, and the culture medium was replaced twice a week until the end of the experiment. Then, the cells were rinsed twice with PBS to remove floating cells, fixed with 4% formaldehyde in PBS for 20 min, and stained with 0.1% crystal violet for 30 min. The staining solution was then removed by aspiration, and the colonies were washed thrice with water and air-dried (Fedele et al., 2018). All experiments were performed at least thrice, and representative results are shown.

2.8 Western blotting

The protein expression of the components of the RAS/ERK pathway was detected in PCC0208023-treated cells by western blotting as previously described (Mainardi et al., 2018; Ahmed et al., 2019). The LS180 and HCT116 cells were plated in a 10-cm diameter dish. After 24 h, the cells were grown in the absence of serum (starvation) overnight. Briefly, 2×10^6 LS180 or HCT116 cells were seeded in 10-cm dishes. When the cells were at 60-70% confluence, they were grown in the absence of serum (starvation) overnight. After starvation, the cells were treated with DMSO (final concentration = 0.1%) or PCC0208023 (1, 5 and 10 μM) for 1 h. The cells were

stimulated with 100 ng/mL of hEGF for 5 min before cell lysis. At the desired time points, the culture medium was immediately removed, and the cells were washed with ice-cold PBS and lysed with RIPA buffer supplemented with protease inhibitors and a phosphatase inhibitor cocktail at 4°C (Yang et al., 2018). Protein concentrations were quantified using a BCA protein assay kit. Total proteins were electrophoresed on 4%–20% GenScript ExpressPlusTM PAGE gel and then transferred onto polyvinylidene fluoride (PVDF) membranes. The membranes were incubated in 5% skimmed milk saline for 2 h at room temperature, and then incubated with primary antibodies against SHP2 (1:1,000), p-SHP2 (1:1,000), ERK1/2 (1:2,000), p-ERK1/2 (1:2,000), MEK1/2 (1:1,000), p-MEK1/2 (1:1,000), and GAPDH (1:2,000) overnight at 4°C. Then, the immunoreactive bands were hybridized with horseradish peroxidase (HRP)-conjugated secondary antibodies of the same species source for 2 h at room temperature. Chemiluminescent signals were detected using an enhanced chemiluminescence kit. The quantification of protein bands were conducted by using Image J software.

2.9 RAS activation assay

Active RAS (RAS-GTP) was pulled down from LS180 and HCT116 cells. The cells were cultured according to the method in section 2.8. After overnight serum starvation and treatment with DMSO (final concentration = 0.1%) or PCC0208023 (1, 5, 10 µM) for 1 h. The cells were stimulated with 100 ng/mL hEGF for 5 min before cell lysis. Following protein extraction and quantification, the glutathione S-transferase–RBD fusion protein (GST–RBD) assay for RAS activation was performed using RAS

activation assay kit according to the manufacturer's instructions.

2.10 Animals

Female nude mice (BALB/c, 6–8 weeks of age) were obtained from Vital River Laboratory Animal Technology Co., Ltd. Sprague–Dawley (SD) rats (average weight: 200 ± 20 g) were purchased from Jinan Pengyue Laboratory Animal Breeding Co., Ltd. All animals were examined prior to the initiation of studies to ensure that they were healthy and had acclimated to the laboratory environment. The animals were housed in standard laboratory conditions (temperature 22 ± 2 °C, 12-h light/dark cycle, food and water were provided *ad libitum*). The protocol was approved by the Experimental Animal Research Committee of Yantai University (Yantai, China).

2.11 Tumor xenograft experiments

To establish xenograft tumor models, the cells (HCT116: 5×10^6 cells, LS180: 2×10^6 cells) were suspended in 0.1 mL of a 1:1 mixture of RPMI 1640 and Matrigel[®] and injected subcutaneously into the right flank of male nude mice (Ma et al., 2018; Tang et al., 2019). Tumor volume was measured thrice a week. When the size of the tumors reached a volume of roughly $130\text{--}150$ mm³ (10 days after injection) as measured by calipers (volume = $1/2 \times (\text{Length} \times \text{Width}^2)$), the mice were randomly assigned to four groups, each containing six animals: (a) vehicle; (b) 15 mg/kg PCC0208023; (c) 30 mg/kg PCC0208023; and (d) 30 mg/kg RMC-4550. The vehicle was captisol/50 mM sodium acetate buffer (pH 4.6) (10%/90%, w/v%), and PCC0208023 was dissolved in the vehicle at concentrations of 1.5 mg/mL and 3.0 mg/mL. The LS180 and HCT116-bearing mice were administered daily by oral gavage for 17 days and 26

days, respectively. Tumor volume and animal weight were measured thrice a week and continued until termination of the experiments. The day of administration was defined as day 0. The measurement time points of the LS180 tumor model were days 0, 3, 5, 8, 10, 12, 15, and 17, respectively. The measurement time points of the HCT116 tumor model were days 0, 3, 5, 8, 10, 12, 15, 17, 19, 22, 24, and 26, respectively. All mice were euthanized by cervical dislocation at the end of the experiment, and tumors were collected and weighed. The inhibition rate was calculated relative to the vehicle.

2.12 Immunohistochemical analysis

At the end of the tumor xenograft experiments in section 2.11, the collected tumors samples were fixed in 4% paraformaldehyde solution, dehydrated, and embedded in paraffin wax. The paraffin-embedded sections of 4- μm thickness were processed for immunohistochemical staining for Ki67, cleaved caspase-3, and p-ERK as previously described (Sun et al., 2013). Briefly, sections were blocked with 3% normal goat serum and incubated with cleaved caspase-3 (1:500), p-ERK (1:800) and Ki67 (1:1,600) antibodies overnight at 4°C and then incubated with the corresponding biotinylated secondary antibodies. The sections were developed with DAB (3, 3'-diaminobenzidine) and counterstained with hematoxylin. Protein-positive cells exhibited brown staining. Slides were examined under high-power microscopy (200 \times) using a Vectra automated quantitative pathology imaging system (PerkinElmer, Waltham, MA, USA).

2.13 Molecular docking studies

2.13.1 Preparation of protein structure

The X-ray structure of the SHP2 homodimer in complex with SHP099 (PDB code: 5EHR) was obtained from the Protein Data Bank (Chen et al., 2016) and reserved for docking-based studies. All water molecules were cleared, hydrogen atoms were added properly to the complexes, and hydrogen bond formations were well maximized by optimization of key residues.

2.13.2 Preparing the ligand

PCC0208023 and RMC-4550 were sketched in ChemBioDraw and converted into 3D structures followed by a local minimization using an MMFF force field. The resulting structures were used for the following docking simulations.

2.13.3 Docking procedure

First, the protein's geometry was optimized utilizing a fast Dreiding-like force field. The targeted protein was completely checked using the "Clean Geometry" toolkit of DS 2018. Then, 10 replicas for each described compound (PCC02080123 and RMC-4550) were produced as a spherical scope with a diameter of 20Å and centered on the SHP2 adduct. Random conformation was limited to 10, simulated annealing methods were set to true, and other parameters were retained by default. Finally, 10 of the best conformations were saved for further analysis.

2.14 Pharmacokinetics study

LS180 tumor model construction was the same as described in Section 2.11. When the size of the tumors reached a volume of roughly 130–150 mm³, the mice were randomized into 4 groups, each containing 12 animals: (a) vehicle; (b) 10 mg/kg

PCC0208023; (c) 30 mg/kg PCC0208023; and (d) 10 mg/kg RMC-4550. The vehicle was captisol/50 mM sodium acetate buffer (pH 4.6) (10%/90%, w/v%). The drug was consecutively administered for 17 days. At pre-dose and 2, 8, 24 h post-dose after the last dose, 0.5 mL of blood (4/group/time point) and tumor tissues (3/group/time point) were collected. The blood was collected from the retro-orbital plexus into heparinized tubes. Plasma was prepared after centrifugation at 8,000 rpm for 10 min and then stored at -20°C. The tumor tissues were homogenized with saline (1:4, w/v). The concentration of PCC0208023 in the plasma samples and tumor tissues were determined using LC-MS/MS system consisting of Agilent 1100 and TSQ Quantum Access (Thermo Electron Corp., San Jose, CA, USA).

2.15 Tissue distribution study

In tumor-bearing mice, 30 mg/kg of PCC0208023 imparted anti-tumor effects, which were converted to the corresponding rat equivalent dose of 15 mg/kg. Therefore, 15 mg/kg was used to investigate the tissue distribution in SD rats (12 in total, 3 per time point). The above vehicle was used to dissolve PCC0208023 with the concentration of 3 mg/mL. After a single dose by oral gavage, the samples were collected at 0.5, 3, 12, and 24 h post-dose. Blood samples were collected from the suborbital veniplex, and plasma samples were prepared after centrifugation at 8,000 rpm for 10 min. The heart, brain, lung, liver, spleen, kidney, stomach, and intestines were excised, rinsed with saline, and blotted dry. Plasma and tissue samples were stored at -80 °C until analysis. All samples were determined using LC-MS/MS system consisting of Agilent 1100 and TSQ Quantum Access.

2.16 Statistical analysis

For statistical comparisons, GraphPad Prism 5 Software was used with one-way ANOVA and then Dunnett's multiple comparison tests. All experimental results were expressed as the mean \pm SD, unless stated otherwise, and differences with $P < 0.05$ were considered statistically significant between the control and treatment groups.

3. Results

3.1 PCC0208023 was a potent SHP2 allosteric inhibitor

To investigate the impact of PCC0208023 on SHP2, the inhibitory potentials of PCC0208023 on SHP2 activity (full-length and catalytic domain) were studied. **Figure 1A** showed that the half maximal inhibitory concentrations (IC_{50}) of PCC0208023 and RMC-4550 on SHP2 full-length enzyme are 2.10 nM and 4.64 nM, respectively, and both compounds lacked the activity against the free catalytic domain of SHP2 (**Figure 1B**).

Furthermore, the inhibition type of both compounds on full-length SHP2 was investigated. **Figure 1C and 1D** showed that the K_m values are almost the same at different concentrations of PCC0208023 and RMC-4550, whereas the values of V_{max} decreased with the increasing concentration. Their modes of inhibition were characterized as non-competitive. The results thus indicated that PCC0208023 is an allosteric, non-competitive inhibitor of SHP2 enzyme (full-length).

3.2 PCC0208023 suppressed the proliferation of CRC cell lines

To explore the effects of PCC0208023 on KRAS mutant CRC cells, growth inhibition assays were performed with PCC0208023 or RMC-4550 in a panel of KRAS mutant

human CRC cell lines (**Table 1**). PCC0208023 and RMC-4550 exhibited cell growth inhibitory effects when cells were treated for 3, 5 and 7 days. The IC₅₀ values were presented in **Table 2**. The IC₅₀ ratios of RMC-4550 to PCC0208023 were within the range of 3.51–11.36, which indicated that the inhibitory effects of PCC0208023 against CRC cells are superior to RMC-4550.

In the colony formation assays, PCC0208023 significantly inhibited colony formation (**Figure 2A-2D**). In the SW837 cells, the colony formation rates of PCC0208023 at doses of 0.15, 0.50 and 1.5 μ M were 84.88%, 73.76%, and 17.59%, respectively. In the SW1463 cells, the colony formation rates of PCC0208023 at doses of 0.25, 0.50, and 0.75 μ M were 76.33%, 47.34%, and 37.47%, respectively. Based on the above results, we conclude that PCC0208023 has good tumor survival inhibitory effects at the cellular level.

3.3 Effects of PCC0208023 on the RAS/ERK pathway in CRC cells

The effects of PCC0208023 on critical signaling pathways were investigated in LS180 and HCT116 cells (**Figure 3A and 3B**). Compared with the control group, the levels of p-MEK, p-ERK, p-SHP2 and RAS-GTP in the HCT116 and LS180 cells were reduced after PCC0208023 treatment for 1h. These findings confirmed that PCC0208023 decreases RAS/ERK signaling.

3.4 PCC0208023 had a good antitumor activity *in vivo*

Based on the inhibitory effects against KRAS mutant cell lines, we assessed the antitumor efficacy of PCC0208023 in a subcutaneous LS180 xenograft model. Compared with the vehicle, PCC0208023 (15 and 30 mg/kg) and RMC-4550 (30

mg/kg) induced remarkable reductions in tumor weight (**Figure 4A, Table 3**) and retarded tumor growth (**Figure 4B**) on the 17th day of administration. PCC0208023 did not impart any significant effect on mouse body weight, while the animals in the RMC-4550 group exhibited a significant reduction in body weight on the 12th day, followed by recovery during the subsequent treatment (**Figure 4C**). Immunohistochemical analysis showed that after treatment with PCC0208023, the expression of Ki67 and p-ERK in xenograft tumors decreased, whereas the expression of cleaved caspase-3 increased (**Figure 4G**).

We also investigated the anti-tumor efficacy of PCC0208023 in the HCT116 xenograft model. Compared with the vehicle, PCC0208023 (30 mg/kg) and RMC-4550 (30 mg/kg) induced remarkable reductions in tumor weight (**Figure 4D, Table 3**) and retarded tumor growth (**Figure 4E**) on the 26th day of administration. In addition, 30 mg/kg of RMC-4550 and PCC0208023 resulted in significant reductions in body weight on the 8th and 12th days, respectively, followed by recovery during subsequent treatment (**Figure 4F, Table 3**).

3.5 Docking analysis of potential binding modes of PCC0208023 and RMC-4550

To understand the binding modes of PCC0208023 and RMC-4550 in this newly reported allosteric pocket (PDB code: 5EHR), optimal molecular docking (CDOCKER, Discovery Studio 2018) was performed (**Figure 5**). The amine group of PCC0208023 formed the key donor-acceptor polar interaction with Phe113, and a hydrogen bond interaction was observed between the nitrogen atom of pyrazolo [3, 4-b] pyrazine ring and the amine of Arg111. Furthermore, by introducing a sulfur

atom, the 2, 3-dichlorophenyl moiety fitted into the deep hydrophobic region that was formed by Asp489, Leu254, Gln495, and Lys492. From the superimposed complex conformation between PCC0208023 and RMC-4550, we found that RMC-4550 could not interact with Phe113 to form the key hydrogen bond, and the molecular stretching direction of PCC0208023 is more stable.

3.6 Pharmacokinetics and tissue distribution profiles

We measured the concentrations of PCC0208023 in the plasma and tumors of the LS180 model mice (**Figure 6A** and **6B**). In plasma and tumors, drug concentrations increased with the increasing doses at 2 h, 8 h, and 24 h, respectively. At 10 mg/kg, the plasma concentration of PCC0208023 was lower than RMC-4550 at 2 h, 8 h or 24 h. And the tumor concentration of PCC0208023 was lower than RMC-4550 at 2 h post-dose, while the concentrations of both compounds were similar at 8 h and 24 h.

In the tissue distribution study, the concentrations of PCC0208023 in the tissue and plasma of rats were measured after a single dose of 15 mg/kg. The concentration-time histograms of PCC0208023 in the several organs are shown in **Figure 6C**. The concentrations of PCC0208023 in plasma were significantly lower than those in the liver, spleen, lung, kidney, and intestines. Among these organs, high tissue distribution in the lung and intestines were found. At 0.5, 3, 12, and 24 h after administration, the respective mean concentrations of PCC0208023 in the lungs were 9.89, 42.48, 36.60, and 6.73 $\mu\text{mol/kg}$, and in the intestines were 82.27, 57.13, 5.75, and 1.94 $\mu\text{mol/kg}$.

4 Discussion

Colorectal cancer (CRC) is one of the most common life-threatening malignancies

worldwide (Obuch and Ahnen, 2016; Rampado et al., 2019), and KRAS mutations are the most common genetic variation in CRC. SHP2 is the first discovered oncogenic tyrosine phosphatase that plays an essential role in oncogenic KRAS-driven tumors (Ruess et al., 2018). SHP2 allosteric inhibitors are an essential part of molecules with high therapeutic potential for cancer treatment. Here, we synthesized PCC0208023 and evaluated its inhibitory effects against SHP2 enzyme, and the KRAS mutant CRC *in vitro* and *in vivo*, and the RAS/MAPK signaling pathway. Consistent with an allosteric mode of inhibition, PCC0208023 can non-competitively inhibit the activity of full-length wild-type SHP2 enzyme, and its inhibitory activity is better than RMC-4550, but both lack activities against the free catalytic domain of SHP2. Furthermore, in KRAS mutant CRC cells, PCC0208023 was more effective in inhibiting cell proliferation than RMC-4550 *in vitro*. Molecule docking assays indicated that the amine group of PCC0208023 engages in additional donor-acceptor polar interactions with F115 than RMC-4550. This may be the reason why PCC0208023 exhibits better inhibitory activity than RMC-4550 in SHP2 full-length enzyme and KRAS mutant CRC cells.

SHP2 has an activating effect on the RAS/ERK signaling pathway to promote cancer cell survival and proliferation (Vazhappilly et al., 2018). In the present study, PCC0208023 significantly reduced the expression of p-MEK and p-ERK in LS180 and HCT116 cells. Our research implied that PCC0208023 may exert anti-tumor effects by inhibiting the RAS/ERK signaling pathway. These findings are in line with those already obtained in a previous study, which demonstrated that SHP2 inhibitor

treatment decreases oncogenic RAS/MAPK signaling in cancer cell lines that are driven by KRAS mutations (Nichols et al., 2018).

We further explored the *in vivo* anti-tumor activity of PCC0208023 using the LS180 and HCT116 xenograft models. At the same dose, PCC0208023 and RMC-4550 produced similar anti-tumor growth effects by significantly reducing tumor weight and tumor volume. Of note, anti-tumor effects are reflected by the expression levels of Ki67, cleaved caspase-3, and p-ERK. Ki67 is a cancer antigen and is a useful marker for cell proliferation (Inwald et al., 2013; Sun et al., 2018). ERK, as the critical intermediate in the MAPK signaling pathway, is classically known as an important regulator of cell proliferation, differentiation, and survival by regulating gene expression (Dhillon et al., 2007). PCC0208023 significantly reduced the expression of Ki67 and p-ERK in tumors, indicating that PCC0208023 could effectively inhibit tumor cell proliferation. Cleaved caspase-3, which is involved in the activation cascade of caspases responsible for apoptosis execution (Bernard et al., 2019), and the treatment with PCC0208023 significantly increased the expression levels of cleaved caspase-3, suggesting that PCC0208023 could induce apoptosis of tumor cells.

Next, we evaluated the pharmacokinetics and tissue distribution profiles of PCC0208023 *in vivo*. At a dose of 10 mg/kg, the tumor concentration of PCC0208023 was lower than RMC-4550 at 2 h post-dose, while the concentrations of both compounds were similar at 8 h or 24 h. This may be the reason why PCC0208023 has comparable efficacy to RMC-4550 for *in vivo* studies. Moreover, tissue distribution

experiments in rats revealed that PCC0208023 is mainly distributed in the intestines and lungs. These findings indicated that PCC0208023 may be potentially utilized as an SHP2 inhibitor for the treatment of CRC and lung cancer.

In conclusion, we have demonstrated that PCC0208023 acts as a potent allosteric inhibitor and suppresses the growth of KRAS mutant colorectal cancer *in vitro* and *in vivo* by inhibiting the SHP2/RAS/ERK signaling pathway. Further optimization of PCC0208023 to identify more low-toxic and potent SHP2 allosteric inhibitors with novel scaffolds for treating KRAS mutation-positive CRC are warranted.

Author contributions

Xiao Chen and Fangxia Zou: Conceptualization, Methodology, Software, Writing-Original draft preparation. Zhenqiang Hu, Guangying Du and Pengfei Yu: Visualization, Investigation. Wenyun Wang and Hongbo Wang: Software, Validation. Liang Ye and Jingwei Tian: Supervision, Writing- Reviewing and Editing.

Funding

This work was supported by the National Natural Science Foundation of China (Grant NO. 81473188), the Key Project of Shandong Province (Grant No.2017GSF218106), Taishan Industry Leading Talent Laureate and the Major New Drugs Research & Development special projects of Ministry of Science and Technology of PR China (NO. 2018ZX09303015).

Competing interests: The authors declare that there are no conflicts of interest

References

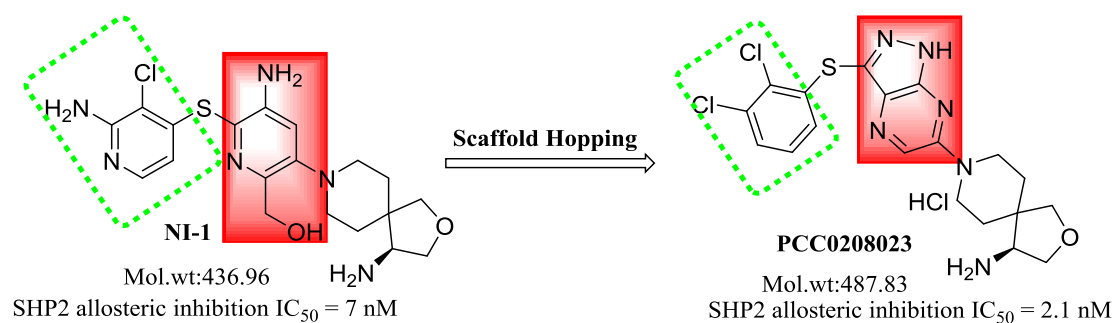
- Ahmed, T.A., Adamopoulos, C., Karoulia, Z., Wu, X., Sachidanandam, R., Aaronson, S.A., Poulikakos, P.I., 2019. SHP2 drives adaptive resistance to ERK signaling inhibition in molecularly defined subsets of ERK-dependent tumors. *Cell Rep.* 26, 65-78. <https://doi.org/10.1016/j.celrep.2018.12.013>.
- Bernard, A., Chevrier, S., Beltjens, F., Dosset, M., Viltard, E., Lagrange, A., Derangère, V., Oudot, A., Ghiringhelli, F., Collin, B., Apetoh, L., Feron, O., Chen, S., Arnould, L., Végran, F., Boidot, R., 2019. Cleaved Caspase-3 transcriptionally regulates angiogenesis-promoting chemotherapy resistance. *Cancer Res.* 79, 5958-5970. <https://doi.org/10.1158/0008-5472>.
- Bray, F., Ferlay, J., Soerjomataram, I., Siegel, R.L., Torre, L.A., Jemal, A., 2018. Global cancer statistics 2018: globocan estimates of incidence and mortality worldwide for 36 cancers in 185 countries. *CA Cancer J Clin.* 68, 394-424. <https://doi.org/10.3322/caac.21492>.
- Canon, J., Rex, K., Saiki, A. Y., Mohr, C., Cooke, F., Dogal, D., Gaida, K., Holt, T., Knutson, C.G., Koppada, N., Lanman, B.A., Werner, J., Rapaport, A.S., San Miguel, T., Ortiz, R., Osgood, T., Sun, J.P., Zhu, X., McCarter, J.D., Volak, L.P., Houk, B.E., Fakih, M.G., O'Neil, B.H., Price, T.J., Falchook, G.S., Desai, J., Kuo, J., Govindan, R., Hong, D., Qiyang, W., Henary, H., Arvedson, T., Cee, V.J., Lipford, J.R., 2019. The clinical KRAS (G12C) inhibitor AMG 510 drives anti-tumour immunity. *Nature.* 575, 217-223. <https://doi.org/10.1038/s41586-019-1694-1>.
- Chen, C.H., CHEN, Z., Dore, M., Fortanet, J.G., Karki, R., Kato, M., LAMARCHE, M.J., PEREZ, L.B., SMITH, T.D., WILLIAMS, S., SENDZIK, M., 2015. N-azaspirocycloalkane substituted N-heteroaryl compounds and compositions for inhibiting the activity of SHP2. WO Patent 2015107495(A1).
- Chen, Y.N., Lamarche, M.J., Chan, H.M., Fekkes, P., Garcia-Fortanet, J., Acker, M.G., Antonakos, B., Chen, C.H., Chen, Z., Cooke, V.G., Dobson, J.R., Deng, Z., Fei, F., Firestone, B., Godor, M., Fridrich, C., Gao, H., Grunfelder, D., Hao, H.X., Jacob, J., He, S., Hsiao, K., Kang, Z.B., Karki, R., Kato, M., Larrow, J., La Bonte, L.R., Lenoir, F., Liu, G., Liu, S., Majumdar, D., Meyer, M.J., Palermo, M., Perez, L., Pu, M., Price, E., Quinn, C., Shakya, S., Shultz, M.D., Slisz, J., Venkatesan, K., Wang, P., Warmuth, M., Williams, S., Yang, G., Yuan, J., Zhang, J.H., Zhu, P., Ramsey, T., Keen, N.J., Sellers, W.R., Stams, T., Fortin, P.D., 2016. Allosteric inhibition of SHP2 phosphatase inhibits cancers driven by receptor tyrosine kinases. *Nature.* 535, 148-152. <https://doi.org/10.1038/nature18621>.
- ClinicalTrials.gov, 1997. NCT03114319. Dose Finding Study of TNO155 in Adult Patients With Advanced Solid Tumors. <https://clinicaltrials.gov/ct2/show/NCT03114319?cond=TNO-155&draw=2&rank=2>. (accessed 14 April 2017).
- ClinicalTrials.gov, 1997. NCT03518554. A First in Human, Dose Escalation Study of JAB-3068 (SHP2 Inhibitor) in Adult Patients With Advanced Solid Tumors.

- <https://clinicaltrials.gov/ct2/show/NCT03518554?cond=JAB-3068&draw=2&rank=2>. (accessed 8 May 2018).
- ClinicalTrials.gov, 1997. NCT03989115. Dose-Escalation and Dose-Expansion of RMC-4630 and Cobimetinib in Relapsed/Refractory Solid Tumors. <https://clinicaltrials.gov/ct2/show/NCT03989115>. (accessed 18 June 2019).
- Cox, A.D., Fesik, S.W., Kimmelman, A.C., Luo, J., Der, C.J., 2014. Drugging the undruggable RAS: mission possible? *Nat Rev Drug Discov.* 13, 828-851. <https://doi.org/10.1038/nrd4389>.
- Dhillon, A.S., Hagan, S., Rath, O., Kolch, W., 2007. MAP kinase signalling pathways in cancer. *Oncogene.* 26, 3279-3290. <https://doi.org/10.1038/sj.onc.1210421>.
- Fedele, C., Ran, H., Diskin, B., Wei, W., Jen, J., Geer, M.J., Araki, K., Ozerdem, U., Simeone, D.M., Miller, G., Neel, B.G., Tang, K.H., 2018. SHP2 inhibition prevents adaptive resistance to MEK inhibitors in multiple cancer models. *Cancer Discov.* 8, 1237-1249. <https://doi.org/10.1158/2159-8290.CD-18-0444>.
- Grossmann, K.S., Rosário, M., Birchmeier, C., Birchmeier, W., 2010. The tyrosine phosphatase Shp2 in development and cancer. *Adv Cancer Res.* 106, 53-89. [https://doi.org/10.1016/S0065-230X\(10\)06002-1](https://doi.org/10.1016/S0065-230X(10)06002-1).
- Hallin, J., Engstrom, L. D., Hargis, L., Calinisan, A., Aranda, R., Briere, D. M., Sudhakar, N., Bowcut, V., Baer, B.R., Ballard, J.A., Burkard, M.R., Fell, J.B., Fischer, J.P., Vigers, G.P., Xue, Y., Goto, S., Fernandez-Banet, J., Pavlicek, A., Velastagui, K., Chao, R.C., Barton, J., Pierobon, M., Baldelli, E., Patricoin, E.F., Cassidy, D.P., Marx, M.A., Rybkin, I.I., Johnson, M.L., Ou, S.I., Lito, P., Papadopoulos, K.P., Jänne, P.A., Olson, P., Christensen, J.G., 2019. The KRAS (G12C) inhibitor MRTX849 provides insight toward therapeutic susceptibility of KRAS-mutant cancers in mouse models and patients. *Cancer Discov.* 10, 54-71. <https://doi.org/10.1158/2159-8290.CD-19-1167>.
- Inwald, E.C., Klinkhammer-Schalke, M., Hofstädter, F., Zeman, F., Koller, M., Gerstenhauer, M., Ortmann, O., 2013. Ki-67 is a prognostic parameter in breast cancer patients: results of a large population-based cohort of a cancer registry. *Breast Cancer Res Treat.* 139, 539-552. <https://doi.org/10.1007/s10549-013-2560-8>.
- Jogalekar, A., Won, W., Koltun, E. S., Gill, A., Mellem, K., Aay, N., Buckl, A., Semko, C., Kiss, G., 2018. 2, 5-Disubstituted 3-methyl pyrazines and 2,5,6-trisubstituted 3-methyl pyrazines as allosteric SHP2 inhibitors. WO Patent WO2018013597 (A1).
- Lee, J.H., Yun C.W., Han, Y.S., Kim, S., Jeong, D., Kwon, H.Y., Kim, H., Baek, M.J., Lee, S.H., 2018. Melatonin and 5-fluorouracil co-suppress colon cancer stem cells by regulating cellular prion protein-Oct4 axis. *J Pineal Res.* 65, e12519. <https://doi.org/10.1111/jpi.12519>.
- Li, F., Liu, Z., Sun, H., Li, C., Wang, W., Ye, L., Yan, C., Tian, J., Wang, H., 2019. PCC0208017, a novel small-molecule inhibitor of MARK3/MARK4, suppresses glioma progression in vitro and in vivo. *Acta Pharm Sin B.* 10, 289-300. <https://doi.org/10.1016/j.apsb.2019.09.004>.
- Liang, X., Shen, J., 2019. Impact of KRAS mutation status on outcomes of metastatic

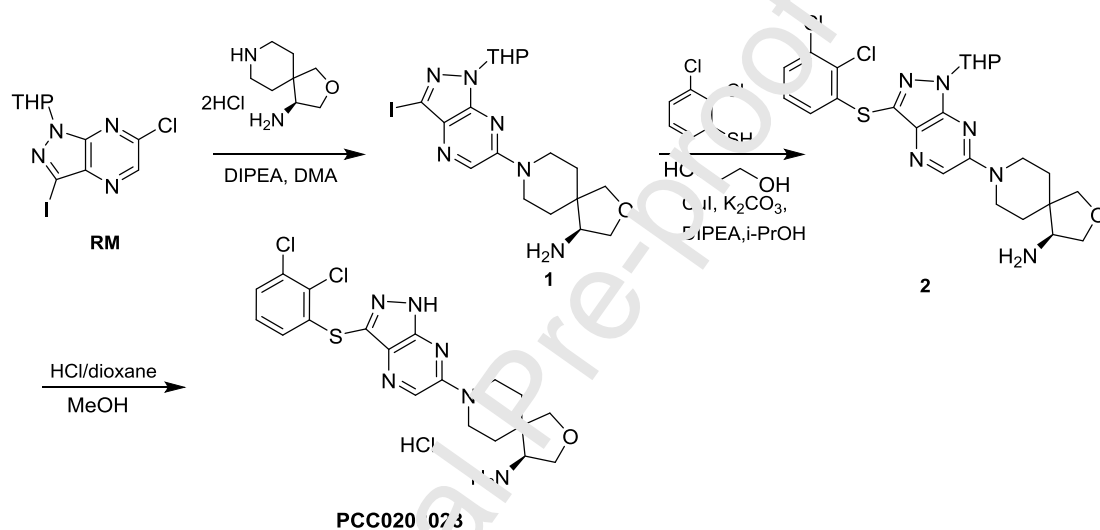
- colorectal cancer treated with anti-angiogenic agents: a meta-analysis. *J Chemother.* 32, 41-48. <https://doi.org/10.1080/1120009X.2019.1692282>.
- Lito, P., Solomon, M., Li, L.S., Hansen, R., Rosen, N., 2016. Allele-specific inhibitors inactivate mutant KRAS G12C by a trapping mechanism. *Science.* 351, 604-608. <https://doi.org/10.1126/science.aad6204>.
- Lv, G., Sun, D., Zhang, J., Xie, X., Wu, X., Fang, W., Tian, J., Yan, C., Wang, H., Fu, F., 2017. Lx2-32c, a novel semi-synthetic taxane, exerts antitumor activity against prostate cancer cells in vitro and in vivo. *Acta Pharm Sin B.* 7, 52-58. <https://doi.org/10.1016/j.apsb.2016.06.005>.
- Ma, Y.T., Yang, Y., Cai, P., Sun, D.Y., Sánchez-Murcia, P.A., Zhang, X.Y., Jia, W.Q., Lei, L., Guo, M., Gago, F., Wang, H., Fang, W.S., 2018. A series of enthalpically optimized docetaxel analogues exhibiting enhanced antitumor activity and water solubility. *J Nat Prod.* 81, 524-533. <https://doi.org/10.1021/acs.jnatprod.7b00857>.
- Mai, T.T., Lito, P., 2018. A treatment strategy for KRAS-driven tumors. *Nat Med.* 24, 902-904. <https://doi.org/10.1038/s41591-018-0111-x>.
- Mainardi, S., Mulero-Sánchez, A., Prahallad, A., Germano, G., Bosma, A., Krimpenfort, P., Liefink, C., Steinberg, J.D., de Wit, N., Gonçalves-Ribeiro, S., Nadal, E., Bardelli, A., Villanueva, A., Bernards, R., 2018. SHP2 is required for growth of KRAS-mutant non-small-cell lung cancer in vivo. *Nat Med.* 24, 961-967. <https://doi.org/10.1038/s41591-018-0023-9>.
- Matozaki, T., Murata, Y., Saito, Y., Okajawa, H., Ohnishi, H., 2009. Protein tyrosine phosphatase SHP-2: a proto-oncogene product that promotes Ras activation. *Cancer Sci.* 100, 1786-1793. <https://doi.org/10.1111/j.1349-7006.2009.01257.x>.
- Nichols, R.J., Haderk, F., Samlhub, C., Schulze, C.J., Hemmati, G., Wildes, D., Tzitzilonis, C., Motdec, K., Marquez, A., Romero, J., Hsieh, T., Zaman, A., Olivas, V., McCoach, C., Blakely, C.M., Wang, Z., Kiss, G., Koltun, E., Gill, A.L., Singh, M., Goldsmith, M.A., Smith, J.A.M., Bivona, T.G., 2018. RAS nucleotide cycling underlies the SHP2 phosphatase dependence of mutant BRAF-, NR1-, and RAS-driven cancers. *Nat Cell Biol.* 20, 1064-1073. <https://doi.org/10.1038/s41556-018-0169-1>.
- Nussinov, R., Tsai, C.J., Jang, H., 2019. Oncogenic KRas mobility in the membrane and signaling response. *Semin Cancer Biol.* 54, 109-113. <https://doi.org/10.1016/j.semcancer.2018.02.009>.
- Obuch, J.C., Ahnen, D.J., 2016. Colorectal Cancer: Genetics is Changing Everything. *Gastroenterol Clin North Am.* 45, 459-476. <https://doi.org/10.1016/j.gtc.2016.04.005>.
- Pylayeva-Gupta, Y., Grabocka, E., Bar-Sagi, D., 2011. RAS oncogenes: weaving a tumorigenic web. *Nat Rev Cancer.* 11, 761-774. <https://doi.org/10.1038/nrc3106>.
- Rampado, R., Crotti, S., Caliceti, P., Pucciarelli, S., Agostini, M., 2019. Nanovectors Design for Theranostic Applications in Colorectal Cancer. *J Oncol.* 2019, 2740923. <https://doi.org/10.1155/2019/2740923>.

- Ran, H., Tsutsumi, R., Araki, T., Neel, B.G., 2016. Sticking it to cancer with molecular glue for SHP2. *Cancer Cell* 30, 194-196. <https://doi.org/10.1016/j.ccell.2016.07.010>.
- Ruess, D.A., Heynen, G.J., Ciecieski, K.J., Ai, J., Berninger, A., Kabacaoglu, D., Görgülü, K., Dantes, Z., Wörmann, S.M., Diakopoulos, K.N., Karpathaki, A.F., Kowalska, M., Kaya-Aksoy, E., Song, L., van der Laan, E.A.Z., López-Alberca, M.P., Nazaré, M., Reichert, M., Saur, D., Erkan, M.M., Hopt, U.T., Sainz, B. Jr., Birchmeier, W., Schmid, R.M., Lesina, M., Algül, H., 2018. Mutant KRAS-driven cancers depend on PTPN11/SHP2 phosphatase. *Nat Med* 24, 954-960. <https://doi.org/10.1038/s41591-018-0024-8>.
- Shi, F., Li, T., Liu, Z., Qu, K., Shi, C., Li, Y., Qin, Q., Cheng, L., Jin, X., Yu, T., Di, W., Que, J., Xia, H., She, J., 2018. FOXO1: another avenue for treating digestive malignancy? *Semin Cancer Biol* 50, 124-131. <https://doi.org/10.1016/j.semcancer.2017.09.009>.
- Sun, S., Du, G., Xue, J., Ma, J., Ge, M., Wang, H., Fan, J., 2018. PCC0208009 enhances the anti-tumor effects of temozolomide through direct inhibition and transcriptional regulation of indoleamine 2,3-dioxygenase in glioma models. *Int J Immunopathol Pharmacol* 32, 2058738418787991. <https://doi.org/10.1177/2058738418787991>.
- Tang, M., Svirskis, D., Leung, E., Kananak, M., Wang, H., Wu, Z., 2019. Can intracellular drug delivery using hyaluronic acid functionalised pH-sensitive liposomes overcome gemcitabine resistance in pancreatic cancer? *J Control Release* 305, 89-100. <https://doi.org/10.1016/j.jconrel.2019.05.018>.
- Torres-Ayuso, P., Brognard, J., 2018. Shipping out MEK inhibitor resistance with SHP2 inhibitors. *Cancer Discov* 8, 1210-1212. <https://doi.org/10.1158/2155-8290.CD-18-0915>.
- Vazhappilly, C.G., Saleh, E., Ramadan, W., Menon, V., Al-Azawi, A.M., Tarazi, H., Abdu-Allah, H., El-Sorbagi, A.N., El-Awady, R., 2018. Inhibition of SHP2 by new compound induces differential effects on RAS/RAF/ERK and PI3K/AKT pathways in different cancer cell types. *Invest New Drugs* 37, 252-261. <https://doi.org/10.1007/s10637-018-0626-5>.
- Yang, Y., Guan, D., Lei, L., Lu, J., Liu, J. Q., Yang, G., Yan, C., Zhai, R., Tian, J., Bi, Y., Fu, F., Wang, H., 2018. H6, a novel hederagenin derivative, reverses multidrug resistance in vitro and in vivo. *Toxicol Appl Pharmacol* 341, 98-105. <https://doi.org/10.1016/j.taap.2018.01.015>.
- Zhang, J., Zhang, F., Niu, R., 2015. Functions of Shp2 in cancer. *J Cell Mol Med* 19, 2075-2083. <https://doi.org/10.1111/jcmm.12618>.

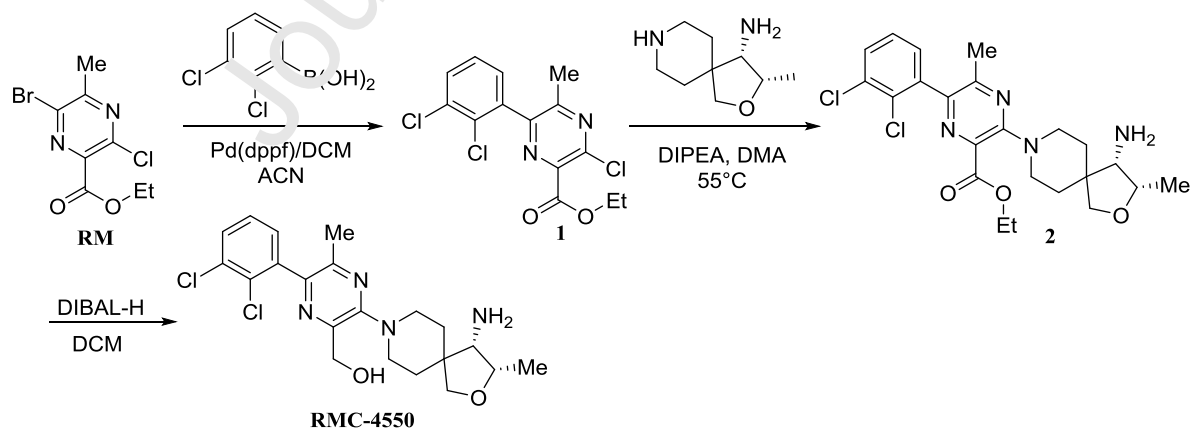
Schemes



Scheme 1 The design process of PCC0208023.



Scheme 2 The synthetic route of PCC0208023.



Scheme 3 The synthetic route of RMC-4550.

Tables

Table 1 KRAS mutant cancer cell lines and mutation status.

Cell lines	Tissue	Gene	CDS change	Amino acid change
HCT116	colon	KRAS	c.38G>A	p.G13D
LS180	colon	KRAS	c.35G>A	p.G12D
SW1463	rectum	KRAS	c.34G>T	p.G12C
SW837	rectum	KRAS	c.34G>T	p.G12C

Table 2 The inhibitory effects of PCC0208023 and RMC-4550 on CRC cells.

Tested compounds	Time (Days)	IC ₅₀ (μM)			
		LS180	HCT116	SW1463	SW837
PCC0208023	3	2.97 ± 0.75	2.00 ± 0.71	1.84 ± 0.40	6.56 ± 2.12
	5	1.92 ± 0.17	0.92 ± 0.18	0.39 ± 0.07	4.84 ± 0.46
	7	2.19 ± 0.61	1.26 ± 0.55	0.77 ± 0.09	3.04 ± 0.26
RMC-4550	3	28.67 ± 6.83	17.56 ± 7.91	7.22 ± 2.00	23.06 ± 5.68
	5	17.16 ± 0.94	10.45 ± 1.22	4.85 ± 0.88	20.64 ± 3.54
	7	17.01 ± 3.59	14.25 ± 4.64	5.73 ± 1.27	21.71 ± 1.35
IC ₅₀ ratios of RMC-4550 to PCC0208023	3	9.65	8.73	3.92	3.51
	5	8.94	11.36	8.22	4.26
	7	7.77	11.34	7.44	7.1

Table 3 Effects of PCC0208023 on body weight and LS180/HCT116 tumor weight.

Tumor model	Group (mg/kg)	Number (initial/ending)	Body weight(g)		Tumor weight (g)	
			Initial ^a	Terminate experiment ^b	g	IR (%)
LS180	Vehicle	6/6	20.23 ± 0.63	20.20 ± 0.99	2.13 ± 0.64	
	PCC0208023 15 mg/kg	6/6	20.58 ± 1.25	19.66 ± 1.88	0.92 ± 0.36*	56.81
	PCC0208023 30 mg/kg	6/6	20.93 ± 0.75	18.90 ± 0.78	0.84 ± 0.22*	60.56
	RMC-4550 30 mg/kg	6/6	20.04 ± 0.50	18.57 ± 0.66	0.69 ± 0.39*	67.61
HCT116	Vehicle	6/6	20.00 ± 0.48	20.11 ± 1.46	2.43 ± 0.76	
	PCC0208023 15 mg/kg	6/6	19.87 ± 0.68	18.70 ± 2.20	1.88 ± 0.59	22.63
	PCC0208023 30 mg/kg	6/6	19.80 ± 0.56	21.25 ± 1.30	1.44 ± 0.41*	40.74
	RMC-4550 30 mg/kg	5/6	19.93 ± 0.72	20.96 ± 0.30	1.33 ± 0.40*	45.27

Note. ^a, Body weight at the time of grouping. ^b, Body weight on the 17th day in the LS180 tumor model and on the 26th day in HCT116 tumor model. * $P < 0.05$, compared with the vehicle group.

Figure legends

Figure 1. PCC0208023 is a non-competitive inhibitor of SHP2. **(A)** The effect of PCC0208023 and RMC-4550 on the enzyme activity of full-length SHP2. **(B)** The effect of PCC0208023 and RMC-4550 on the enzyme activity of the SHP2 catalytic domain. **(C)** Non-competitive inhibition of PCC0208023 on full-length SHP2. **(D)** Non-competitive inhibition of RMC-4550 on full-length SHP2.

Figure 2. Effects of PCC0208023 on colony formation in CRC cells. **(A)** SW837 cells were cultured with the indicated concentration of PCC0208023 for 15 days. **(B)** SW1463 cells were cultured with the indicated concentration of PCC0208023 for 21 days. **(C)** Number of clones formed by SW837 cells. **(D)** Number of clones formed by SW1463 cells. The data are expressed as the mean \pm SD (n = 3). **P* < 0.05 compared with the control.

Figure 3. PCC0208023 suppresses the RAS/ERK pathway. **(A, B)** Western blotting analysis of the expression of RAS-GTP, p-MEK, p-ERK, and p-SHP2 in HCT116 and LS180 cells treated with PCC0208023 (1, 5, and 10 μ M) for 1 hour. The data are expressed as the mean \pm SD (n=3). **P* < 0.05 compared with the control group.

Figure 4. Antitumor effects of PCC0208023 in KRAS-mutant CRC xenograft tumor models. **(A)** Tumor weight of LS180 after 17 d of treatment. **(B)** Tumor growth curve showing tumor growth inhibition (TGI) of PCC0208023 and RMC-4550 in the LS180 model. **(C)** Body weight curve of LS180 xenograft tumor model. **(D)** Tumor weight of HCT116 at death after 26 d of treatment. **(E)** Tumor growth curve showed TGI of PCC0208023 and RMC-4550 in the HCT116 model. **(F)** Body weight curve of the

HCT116 xenograft tumor model. One nude mouse in the RMC4550 group died before tumor removal. The data from Figure 4 A-F are expressed as the mean \pm SD (n = 6 or 5). * $P < 0.05$, compared with the vehicle group. (G) Ki67, cleaved caspase-3 and p-ERK expression levels in three LS180 tumors from each group were analyzed by immunohistochemical analysis.

Figure 5. Molecular docking of PCC0208023 and RMC-4550 with the SHP2 protein.

(A) Two-dimensional (2D) butt conformation of PCC0208023. (B) 2D butt conformation of RMC-4550. (C) Docking modes of PCC0208023 with SHP2 (PDB code: 5EHR). (D) Representative molecular overlap of PCC0208023 and RMC-4550. Key residues are depicted in gray, and hydrogen bonds are represented by dashed green lines.

Figure 6. Pharmacokinetics profiles of PCC0208023. (A) The plasma concentration of PCC0208023 and RMC-4550 in LS180 model mice. The data are expressed as the mean \pm SD (n = 4). (B) The tumor concentration of PCC0208023 and RMC-4550 in LS180 model mice. The data are expressed as the mean \pm SD (n = 3). (C) Concentration-time histograms of PCC0208023 in several organs after oral administration of 15 mg/kg PCC0208023. The data are expressed as the mean \pm SD (n = 3).

Highlights

1. PCC0208023, a potent SHP2 allosteric inhibitor, was designed and synthesized.
2. PCC0208023 inhibited KRAS mutant colorectal cancer growth *in vitro* and *in vivo*.
3. PCC0208023 inhibited SHP2/RAS/ERK signaling pathway in colorectal cancer.
4. PCC0208023 was mainly distributed in the tumor and the intestines.
5. PCC0208023 deserves further optimization to find potent SHP2 allosteric inhibitors.

Journal Pre-proof

Declaration of interests

The authors declare that they have no known competing financial interests or personal relationships that could have appeared to influence the work reported in this paper.

The authors declare the following financial interests/personal relationships which may be considered as potential competing interests:

Journal Pre-proof